

A Monte Carlo method to estimate cell population heterogeneity

Ben Lambert^{1,2*}, David J. Gavaghan³, Simon Tavener⁴.

1 Department of Zoology, University of Oxford, Oxford, Oxfordshire, U.K.

2 MRC Centre for Global Infectious Disease Analysis, School of Public Health, Imperial College London, London W2 1PG, UK.

3 Department of Computer Science, University of Oxford, Oxford, U.K.

4 Department of Mathematics, Colorado State University, Fort Collins, Colorado, U.S.A.

*ben.c.lambert@gmail.com.

Revision date & time: 2019-06-20 02:59

1 Abstract

1
2
3
4
5
6
7
8
9
10
11
12
13
14
15
16
17
18
19
20
21
22
23
24

Variation is characteristic of all living systems. Laboratory techniques such as flow cytometry can probe individual cells and, after decades of experimentation, it is clear that even members of genetically identical cell populations can exhibit differences. To understand whether variation is biologically meaningful, it is essential to discern its source. Mathematical models of biological systems are tools that can be used to investigate causes of cell-to-cell variation. From mathematical analysis and simulation of these models, biological hypotheses can be posed and investigated, then parameter inference can determine which of these is compatible with experimental data. Data from laboratory experiments often consist of “snapshots” representing distributions of cellular properties at different points in time, rather than individual cell trajectories. These data are not straightforward to fit using hierarchical Bayesian methods, which require the number of cell population clusters to be chosen *a priori*. Here, we introduce a computational sampling method named “Contour Monte Carlo” for estimating mathematical model parameters from snapshot distributions, which is straightforward to implement and does not require cells be assigned to predefined categories. Our method is appropriate for systems where observed variation is mostly due to variability in cellular processes rather than experimental measurement error, which may be the case for many systems due to continued improvements in resolution of laboratory techniques. In this paper, we apply our method to quantify cellular variation for three biological systems of interest and provide Julia code enabling others to use this method.

2 Introduction

25
26
27
28
29
30
31
32
33
34
35
36
37
38
39
40
41
42
43
44
45
46
47
48
49

Variation, as opposed to homogeneity, is the rule rather than exception in biology. Indeed, without variation, biology as a discipline would not exist, since as evolutionary biologist JBS Haldane wrote, variation is the “raw material” of evolution. The Red Queen Hypothesis asserts organisms must continually evolve in order to survive when pitted against other - also evolving - organisms [1]. A corollary of this hypothesis is that multicellular organisms should evolve cellular phenotypic heterogeneity to allow faster adaptation to changing environments, which may explain the observed variation in a range of biological systems [2]. Whilst cell population variation can confer evolutionary advantages, it can also be costly in other circumstances. In biotechnological processes, heterogeneity in cellular function can lead to reduced yields of biochemical products [3]. In human biology, variation across cells can enable pathologies to develop and also prevents effective treatment, since medical interventions typically aim to steer modal cellular properties and hence fail to influence key subpopulations. For example, cellular heterogeneity helps some cancerous tumours to persist [4] and can make tumours more likely to evolve resistance to chemotherapies [5]. Identifying and quantifying sources of variation in populations of cells is important for wide ranging applications to discern whether the variability is benign or alternatively requires remedy.

Mathematical models are essential tools for understanding cellular systems, whose emergent properties are the result of complex interactions between various actors. Perhaps the simplest flavour of mathematical model used in biological systems is an ordinary differential equation (ODE)

that lumps individual actors into partitions according to structure or function, and seeks to model the mean behaviour of each compartment. Data from population-averaged experimental assays can determine whether such models faithfully reproduce system behaviours and can be used to understand the interactions of various cellular components of complex metabolic, signalling and transcriptional networks. The worth of such models however depends on whether averages mask substantial differences in individual behaviour [6]. In some cases, differences in cellular protein abundances due to biochemical “noise” are not biologically meaningful [7] and the system is well described by average cell behaviour. In others there are functional consequences. For example, a laboratory study demonstrated that subpopulations of clonally-derived hematopoietic progenitor cells with either low or high expression of a particular stem cell marker resulted in different blood lineages [8].

To accommodate cell population heterogeneity in mathematical models, many modelling frameworks are available, each posing different challenges for parameter inference. A recent review is presented in [9]. These approaches include modelling biochemical processes stochastically using reaction-diffusion equations (RDEs), where properties of ensembles of cells are represented by probability distributions which evolve according to chemical master equations. See [10] for a tutorial on RDEs. Alternatively, population balance equations (PBEs) can be used, which determine the dynamics of the “number density” of differing cell types. In PBEs, cell properties are represented as points in \mathbb{R}^n which, in turn, affect their function, including their rate of death and cell division. In a PBE approach, variation in measured quantities results primarily from differing functional properties of heterogeneous cell types and variable initial densities of each type. See [11] for an introduction to PBEs.

Here, we suppose heterogeneity in quantities of interest across cells is generated by idiosyncratic variation in the rates of cellular processes. The modelling approach we follow is similar to that of [12] and is based on an ODE framework. In our model, each cell evolves according to an ODE, with its progression directed by parameters whose value varies between cells. To our knowledge, this flavour of model is unnamed and so, for sake of reference, we call them “heterogenous ODE” models (HODEs). In HODEs, the aim of inference is to estimate distributions of parameter values across cells consistent with observations. A benefit of using HODEs is that these models are computationally straightforward to simulate and, arguably, simpler to parameterise than PBEs. By using HODEs, we assume that most observed variation comes from differences in biological processes across cells, not inherent stochasticity in biochemical reactions within cells as in stochastic RDEs.

Inference for HODEs is problematic due partly to the experimental hurdles involved with generating data of sufficient standard. Unlike models which represent a population by a single scalar ODE, since HODEs are individual-based, they ideally require individual cell data for estimation. A widely-used method for generating such data is flow cytometry, where a large number of cells are streamed individually through a laser beam and, for example, the concentrations of fluorescently-labelled proteins are measured [13]. Other experimental techniques, including Western blotting and cytometric fluorescence microscopy, can also generate single cell measurements [14, 15]. These experimental methods are all however destructive, meaning individual cells are sacrificed during measurement, and observa-

tions at each time point hence represent “*snapshots*” of the underlying population [15]. These snapshots can be described by histograms [12] or density functions [9] fit to measurements of quantities of interest. Since HODEs assume the state of each cell evolves continuously over time, experimental data tracing individual cell trajectories through time constitutes a richer data resource. The demands of obtaining this data are however higher and typically involve either tracking individual cells through imaging methods [16], or trapping cells in a spatial position where they can be monitored over time [17]. These techniques however impose severe restrictions on experimental practices and cannot be used in many circumstances, including for online monitoring of biotechnological processes or analysis of *in vivo* studies. For this reason, “snapshot” data continues to play an important role for determining cell level variability in many applications.

A variety of approaches have been proposed to estimate cellular variability by fitting HODEs to snapshot data. In HODEs, parameter values vary across cells according to a to-be-determined probability distribution, and the solution to the inverse problem requires solving the cell-specific ODE system many times for each individual. The count of cells in experiments typically exceeds $\sim 10^4$ [15], and so approaches where the computational burden scales with this count are usually infeasible. Instead, approaches that approximate raw snapshot data by fitting probability densities to them are typically more efficient and commonly used [12, 15, 18, 19], and we follow this approach here. We now briefly describe the existing approaches for using HODE models to estimate cell population heterogeneity. Hasenauer et al. (2011) present a Bayesian approach to inference for HODEs, which models the input parameter space using an ansatz of a mixture of densities of chosen types. The authors then use their method to reproduce population substructure on synthetic data generated from a model of tumour necrosis factor stimulus. Hasenauer et al. (2014) use mixture models to model subpopulation structure in snapshot data with multiple-start local optimisation employed to maximise the non-convex likelihood, which they then apply to synthetic and real data from signalling pathway models. Loos et al. (2018) also use mixture models to represent subpopulation structure and use maximum likelihood to estimate both within- and between-subpopulation variability, which permits fitting to multivariate output distributions with complex correlation structures. Dixit et al. (2018) assign observations into discrete bins, then choose likelihood distributions using the principle of maximum entropy to estimate cell variability within a Bayesian framework.

Our framework is Bayesian although is distinct from the approach used to fit many dynamic models, since we assume output variation arises from parameter heterogeneity across cells, with no contribution from measurement noise. The approach is hence most suitable when measurement error is minimal. Our method is a two-step Monte Carlo approach which, for reasons described in §3, we call “Contour Monte Carlo” (CMC). Unlike many existing methods, CMC is straightforward to implement and does not require extensive computation time. CMC uses MCMC in its second step to sample from the posterior distribution meaning it does not require ansatz densities. It also does not require the number of cell clusters be chosen beforehand, rather, subpopulations emerge as modes in the posterior parameter distributions. Like [19], CMC can fit multivariate snapshot data and unlike [12], does not use discrete bins to model continuous data. As more experimental techniques elucidating single cell behaviour are developed, interest in models describing measurement snapshots should follow. We

argue that due to its simplicity and generality, CMC can be used to perform
 inference on the proliferation of rich single cell data, and thus, is a useful
 addition to the modeller’s toolkit.

Outline of the paper: In §3, we describe our probabilistic model of the
 inverse problem and detail the CMC algorithm for generating samples from
 the posterior parameter distribution. In §4, we use CMC to estimate cell
 population heterogeneity in three systems of biological interest.

3 Method

In this section, we first develop a probabilistic framework that describes
 our inverse problem, before introducing the CMC algorithm in pseudocode
 (Algorithm 1). We also detail the workflow we have found helpful in using
 CMC to analyse cell snapshot data and suggest practical remedies to issues
 commonly encountered while using this approach (Figure 4). A glossary of
 variable names used in this paper is included as Table 1.

Experimental methods such as flow cytometry measure single cell char-
 acteristics at a given time. Cells are typically destroyed by the measurement
 process, so the data consists of cross-sections or “snapshots” of sampled
 individuals from the population, rather than providing time series for each
 individual cell (Figure 1).

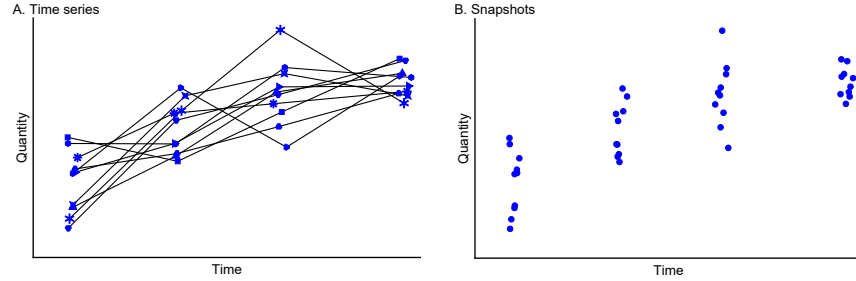


Figure 1: **Data typical of single cell experiments.** **(A)** Time series data. **(B)** Snapshot data. In A, note cell identities are retained at each measurement time (indicated by individual plot markers) whereas in the snapshot data in B, either this information is lost, or more often, cells are destroyed by the measurement process, and each observation corresponds to a distinct cell.

We model the processes of an individual cell using a system of ordinary
 differential equations (ODEs), where each element of the system typically
 corresponds to the concentration of a particular species. Our initial value
 problem is,

$$\begin{aligned} \frac{dx}{dt} &= f(x(t); \theta), & f : \mathbb{R}^k \times \mathbb{R}^p \mapsto \mathbb{R}^k, \\ x(0) &= x_0. \end{aligned} \tag{1}$$

Note that in most circumstances, the initial state of the system, $x(0)$, is
 unknown, and it is convenient to include these as elements of θ to be
 estimated.

3.1 Snapshot data

182
183
184
185

We assume the variation in snapshots arises due to heterogeneity in the underlying parameters θ across cells. Therefore, the evolution of the underlying state of cell i is described by an idiosyncratic ODE,

$$\begin{aligned} \frac{dx^{\{i\}}}{dt} &= f(x^{\{i\}}(t); \theta^{\{i\}}), \quad f : \mathbb{R}^k \times \mathbb{R}^p \mapsto \mathbb{R}^k, \\ x^{\{i\}}(0) &= x_0, \end{aligned} \quad (2)$$

where superscript $\{i\}$ indicates the i th cell. The traditional (non-hierarchical) state-space approach to modelling dynamic systems supposes that measurement error introduces stochastic variation in the output (Figure 2A). Our approach, by contrast, assumes any variation in outputs is solely due to variability in parameter values between cells (Figure 2B). Whether the assumption of “perfect” measurements is reasonable depends on experimental details of the system under investigation, but we argue our method nevertheless provides a useful approximation in cases where the signal to noise ratio is high.

186
187
188
189
190
191
192
193
194

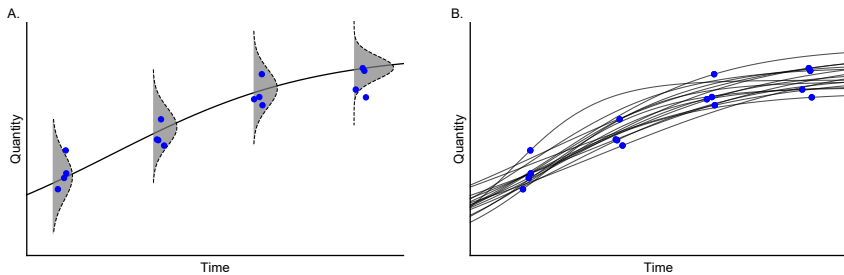


Figure 2: **Models of variation in measured outputs.** (A) **State-space model.** (B) **Parameter heterogeneity model.** (A) For non-hierarchical state-space models, there is a single “true” latent state, and observations result from an imperfect measurement process (grey histograms). (B) For models with parameter heterogeneity, the uncertainty is generated by differences in cellular processes (black lines) between cells. Note that in both cases, individual cells are measured only once in their lifetime.

We suppose m quantities of interest (QOIs) are measured,

$$\mathbf{q}^\top = (q_1, q_2, \dots, q_m) \in \mathbb{R}^m, \quad (3)$$

with n_j observations of each quantity, q_j . Distinct QOIs, q_j , may correspond to different functionals of the solution at the same time or the same functional at different times. The observed data for QOI q_j at the corresponding time t_j consists of the n_j cellular measurements,

$$\mathbf{y}(t_j)^\top = \left(q_j(x^{\{1\}}(t_j)), q_j(x^{\{2\}}(t_j)), \dots, q_j(x^{\{n_j\}}(t_j)) \right) \in \mathbb{R}^{n_j}. \quad (4)$$

The raw snapshot data \mathbf{X} is the collection of all measured QOIs,

$$\mathbf{X} = (\mathbf{y}(t_1), \mathbf{y}(t_2), \dots, \mathbf{y}(t_m)) \in \mathbb{R}^{n_1} \times \mathbb{R}^{n_2} \times \dots \times \mathbb{R}^{n_m}. \quad (5)$$

The goal of inference is to characterise the probability distribution $p(\theta|\mathbf{X})$ representing heterogeneity in the cellular processes. The numbers of cells

196
197
198
199

sampled in typical experimental setups is large and following previous work, we represent snapshot data \mathbf{X} using probability distributions [12, 15, 18, 19]. In the first step of our workflow (Figure 4(i)), these distributions are approximated by a kernel density model, with support over the space of the QOI vector, $\mathbf{q} \in \mathbb{R}^m$. We denote $\hat{\Phi}$ as the parameter estimates of the corresponding kernel density model, $p(\mathbf{q}|\hat{\Phi})$, fitted to raw snapshot data. We assume there are enough observational data that the estimated probability distributions are approximate sufficient statistics of the outputs, meaning $p(\boldsymbol{\theta}|\hat{\Phi}) \approx p(\boldsymbol{\theta}|\mathbf{X})$.

Variable	Definition	Dimension
$\mathbf{x}(t)$	ODE solution	\mathbb{R}^k
$\boldsymbol{\theta}$	ODE parameters	\mathbb{R}^p
$\mathbf{f}(\mathbf{x}(t); \boldsymbol{\theta})$	ODE RHS	\mathbb{R}^k
$\mathbf{x}^{\{i\}}(t)$	ODE solution for cell i	\mathbb{R}^k
$q_j = q_j(\mathbf{x}(t_j); \boldsymbol{\theta}) = q_j(\boldsymbol{\theta})$	quantity of interest (QOI) j	\mathbb{R}^1
$\mathbf{q}^\top = (q_1, \dots, q_m)$	m distinct QOIs	\mathbb{R}^m
$q_j^{\{i\}} = q_j(\mathbf{x}^{\{i\}}(t_j))$	QOI j for cell i	\mathbb{R}^1
$\mathbf{y}_j^\top = (q_j^{\{1\}}, \dots, q_j^{\{n_j\}})$	QOI j for cells $1, \dots, n_j$	\mathbb{R}^{n_j}
$\mathbf{X} = (\mathbf{y}_1, \dots, \mathbf{y}_m)$	“snapshot” of all QOIs	$\mathbb{R}^{n_1} \times \mathbb{R}^{n_2} \times \dots \times \mathbb{R}^{n_m}$
Φ	parametrises output target distribution $p(\mathbf{q} \Phi)$	\mathbb{R}^m
Ξ	parametrises prior parameter distribution $p(\boldsymbol{\theta} \Xi)$	\mathbb{R}^p
Ψ	parametrises prior output distribution $p(\mathbf{q} \Psi)$	\mathbb{R}^p
\hat{a}	estimates of any quantity a	-
$\Omega(\mathbf{z})$	parameter space mapping to $\mathbf{q} = \mathbf{z}$	$\mathbb{R}^{\leq p}$
$\mathcal{V}(\mathbf{z})$	volume of $\Omega(\mathbf{z})$	\mathbb{R}^+
V	volume of (bounded) parameter space	\mathbb{R}^+

Table 1: **Glossary of variable names used in this paper.**

3.2 Theoretical development of CMC

We consider the underdetermined case where $m < p$, so that each specific quantity of interest $\tilde{\mathbf{q}}$ (say) can be generated from a non-singular set of parameter values, which we term iso-output contour regions: $\Omega(\tilde{\mathbf{q}}) = \{\boldsymbol{\theta} : \mathbf{q}(\boldsymbol{\theta}) = \tilde{\mathbf{q}}\}$. In general, these contours have “volumes” $\mathcal{V}(\tilde{\mathbf{q}})$ that depend on the chosen output value $\tilde{\mathbf{q}}$ (Figure 3). Any algorithm that samples parameter values in order to generate a given output target must account for the differential volumes of these sets, otherwise, sampling will be biased towards iso-output contours with larger volumes [20]. The problem in most applied problems however is that we do not know *a priori* the volumes of iso-output contours and so they must be estimated. The following analysis provides a brief introduction to a probabilistic formulation of underdetermined inverse problems (see our companion paper [20] for a more comprehensive discussion). In doing so, this discussion suggests a sampling approach for estimating the volume of parameter space mapping to each output value, which forms the basis of CMC.

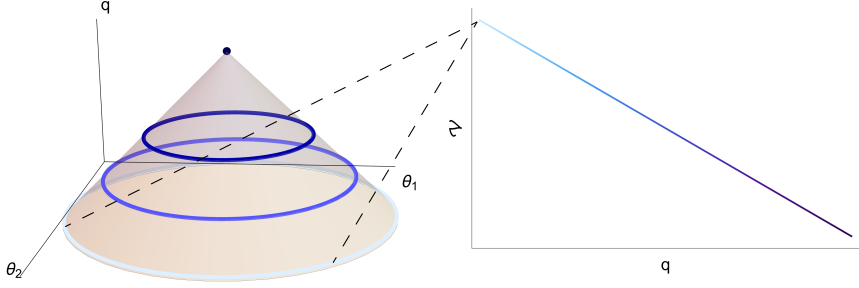


Figure 3: **Left:** An example output function $q(\theta_1, \theta_2)$ along with iso-output contours indicated (coloured lines). **Right:** The “volume” of output contours as a function of output value. Note that here, since the input space is two dimensional, the “volume” of each output value corresponds to a length of an iso-output contour.

Solving our inverse problem requires determining the posterior distribution of parameter values $p(\boldsymbol{\theta}|\hat{\Phi})$ which, when used as input to the forward map, results in the target distribution $p(\mathbf{q}|\hat{\Phi})$. To derive the posterior parameter distribution, we consider the joint density of parameters and QOIs, $p(\boldsymbol{\theta}, \mathbf{q}|\hat{\Phi})$. This can be decomposed in two ways using the law of conditional probability,

$$p(\boldsymbol{\theta}, \mathbf{q}|\Phi) = p(\boldsymbol{\theta}|\mathbf{q}, \Phi) \times p(\mathbf{q}|\Phi) = p(\mathbf{q}|\boldsymbol{\theta}, \Phi) \times p(\boldsymbol{\theta}|\Phi). \quad (6)$$

Rearranging eq. (6) to obtain the posterior parameter distribution,

$$p(\boldsymbol{\theta}|\Phi) = \frac{p(\boldsymbol{\theta}|\mathbf{q}, \Phi) \times p(\mathbf{q}|\Phi)}{p(\mathbf{q}|\boldsymbol{\theta}, \Phi)}. \quad (7)$$

Since the mapping from parameters to outputs is deterministic, $p(\mathbf{q}|\boldsymbol{\theta}, \Phi) = \delta(\mathbf{q}(\boldsymbol{\theta}))$, i.e., the Dirac delta function centred at $\mathbf{q} = \mathbf{q}(\boldsymbol{\theta})$. Thus eq. (7) becomes,

$$p(\boldsymbol{\theta}|\Phi) = p(\boldsymbol{\theta}|\mathbf{q}(\boldsymbol{\theta}), \Phi) \times p(\mathbf{q}(\boldsymbol{\theta})|\Phi). \quad (8)$$

In the same way that a single output value can be caused by any member of a set of parameter values, a target output distribution $p(\mathbf{q}|\Phi)$ can be caused by any member of a set of parameter distributions. To ensure uniqueness of the “posterior” parameter distributions, our probabilistic framework therefore requires that we specify “prior” distributions for the parameters, as in more traditional Bayesian inference. In what follows, we assume the conditional distribution $p(\boldsymbol{\theta}|\mathbf{q}, \Phi)$ is independent of the data, i.e., $p(\boldsymbol{\theta}|\mathbf{q}, \Phi) = p(\boldsymbol{\theta}|\mathbf{q})$, and thus represents a conditional “prior” which can be manipulated using Bayes’ rule as,

$$p(\boldsymbol{\theta}|\mathbf{q}(\boldsymbol{\theta})) = \frac{p(\boldsymbol{\theta})}{p(\mathbf{q}(\boldsymbol{\theta}))}. \quad (9)$$

This results in the form of the posterior parameter distribution targeted by our sampling algorithm,

$$p(\boldsymbol{\theta}|\hat{\Phi}) = \frac{p(\boldsymbol{\theta})}{p(\mathbf{q}(\boldsymbol{\theta}))} p(\mathbf{q}(\boldsymbol{\theta})|\hat{\Phi}). \quad (10)$$

Again, we defer to our companion piece [20] for detailed explanation of eqs. (9) and (10) and, instead, here provide brief interpretation when considering

a uniform prior on parameter space. In this case, $p(\boldsymbol{\theta}) = \frac{1}{V}$, where V is the total volume of parameter space. The denominator term of eq. (9) is the prior induced on output space by the prior over parameter space. For a uniform prior on parameter values, this is,

$$p(\boldsymbol{\theta}|\mathbf{q}(\boldsymbol{\theta})) = \frac{1}{\mathcal{V}(\mathbf{q}(\boldsymbol{\theta}))}, \quad (11)$$

where $\mathcal{V}(\mathbf{q}(\boldsymbol{\theta}))$ is the volume of parameter space occupied by the iso-output contour $\Omega(\mathbf{q}(\boldsymbol{\theta}))$. Therefore, a uniform prior over parameter space implies a prior structure where all parameter values producing the same output are given equal weighting.

3.3 Implementation of CMC

Except for some toy examples, the denominator of eq. (9) cannot be calculated, so exact sampling from the posterior parameter distribution of eq. (10) is not, in general, possible. We propose, instead, a computationally efficient sampling method to estimate $p(\mathbf{q}(\boldsymbol{\theta}))$, which forms the first step of our so-called ‘‘Contour Monte Carlo’’ (CMC) algorithm (Algorithm 1; Figure 4(ii)), where the volume of iso-output contours with each feasible output value is estimated. This step involves repeated independent sampling from the prior distribution of parameters, $\boldsymbol{\theta}^{\{i\}} \sim p(\boldsymbol{\theta}|\Xi)$, where Ξ parameterises the prior probability density. Each parameter sample is then mapped to an output value, $\mathbf{q}^{\{i\}} = \mathbf{q}(\boldsymbol{\theta}^{\{i\}})$. The collection of output samples is then fitted using a vine copula kernel density estimator (KDE) [21], $(\mathbf{q}^{\{1\}}, \dots, \mathbf{q}^{\{N_1\}}) \sim p(\mathbf{q}|\hat{\Psi})$. Throughout the course of development of CMC, we have tested many KDE methods and have found vine copula KDE is best suited to approximating the higher dimensional probability distributions required in practice.

The second step in our algorithm then uses Markov chain Monte Carlo (MCMC) to sample from an approximate version of eq. (10), where the estimated density, $p(\mathbf{q}(\boldsymbol{\theta})|\hat{\Psi})$ replaces its corresponding estimand (Algorithm 1; Figure 4(iii)),

$$p(\boldsymbol{\theta}|\hat{\Phi}, \Xi, \hat{\Psi}) = \frac{p(\boldsymbol{\theta}|\Xi)}{p(\mathbf{q}(\boldsymbol{\theta})|\hat{\Psi})} p(\mathbf{q}(\boldsymbol{\theta})|\hat{\Phi}). \quad (12)$$

The final step in CMC is to compare output samples generated by MCMC with the target distribution (Figure 4(iv)). Asymptotically (in terms of the sample size of both sampling steps), CMC produces a sample of parameter values $(\boldsymbol{\theta}^{\{1\}}, \boldsymbol{\theta}^{\{2\}}, \dots)$ which, when mapped to the output space, corresponds to the target distribution $p(\mathbf{q}|\hat{\Psi})$. In developing CMC, we found that a finite sample of modest size for both steps of CMC results in parameter samples that, when transformed, often represented good approximations of the target. There are, however, occasions when this is not the case, and this final confirmatory step is indispensable since it frequently highlights inadequacies in contour volume estimation or MCMC, meaning more samples from either or both of these steps are required. It may also be necessary to tweak hyperparameters of the KDE in the contour volume estimation step to ensure reasonable approximation of the distribution of output values obtained by sampling the prior density. If the target distribution is sensitive to the contour volume estimates, this may also indicate that the target snapshot distribution is incompatible with the model: here, we make no

claims on existence of a solution to the inverse problem, only that, Contour Monte Carlo is a pragmatic approach to approximate it by sampling if one should exist. A useful way to diagnose whether the target distribution can be produced from the model and chosen priors is to plot the output values from the contour volume estimation step of CMC. If the bulk of target probability mass does not overlap with the simulated output values, then the model and/or chosen prior are unlikely to be invertible to this particular target.

295
296
297
298
299
300
301
302

3.4 Workflow and CMC algorithm

303
304
305
306
307
308

A graphical illustration of the complete CMC workflow is provided in Figure 4. All variables are defined in Table 1. The CMC algorithm is provided in Algorithm 1. For simplicity, in this implementation MCMC sampling is performed via the Random Walk Metropolis algorithm, but for the examples in §4, we use an adaptive MCMC algorithm [22].

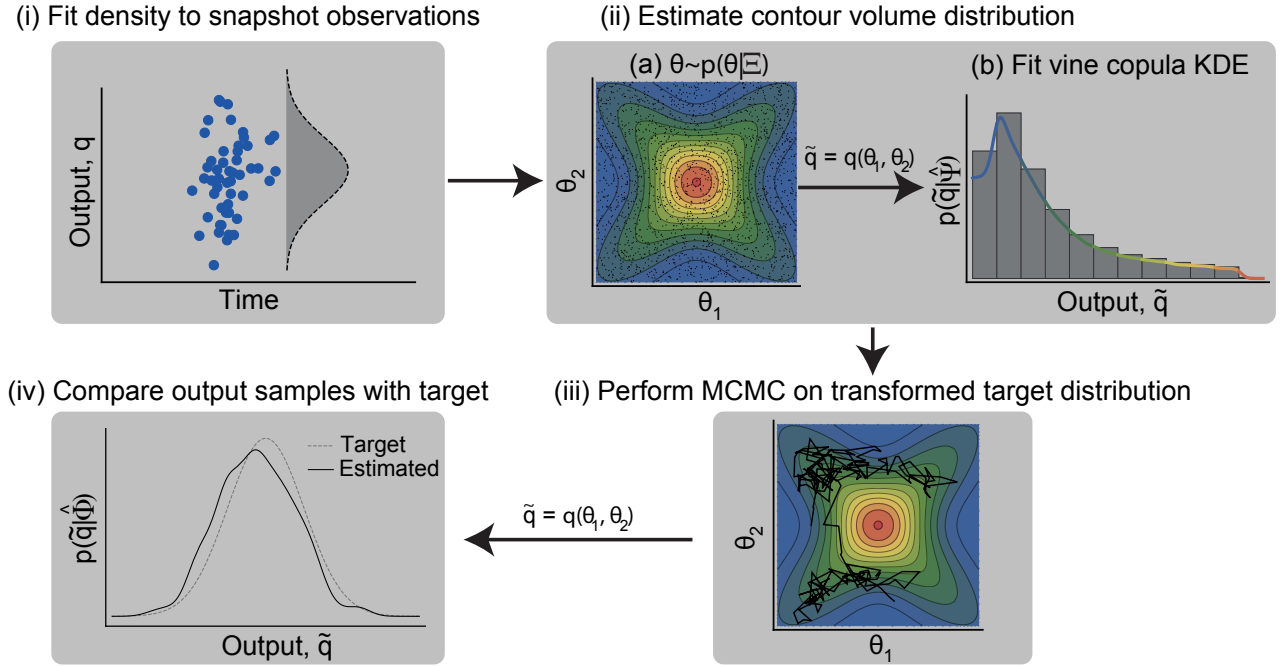


Figure 4: **Workflow for Contour Monte Carlo to estimate cell population heterogeneity.** The distribution targeted in (iii) is given by eq. (12).

Algorithm 1 Pseudocode for the Contour Monte Carlo algorithm for sampling from the posterior parameter distribution of eq. (12).

```

procedure CMC( $\mathbf{X}, \Xi, N_1, N_2$ )       $\triangleright$  Sample from posterior parameter distribution
     $\hat{\Phi} = \text{SNAPSHOTESTIMATOR}(\mathbf{X})$ 
     $\hat{\Psi} = \text{CONTOURVOLUMEESTIMATOR}(\Xi, N_1)$ 
     $(\boldsymbol{\theta}^{\{1\}}, \dots, \boldsymbol{\theta}^{\{N_2\}}) = \text{MCMC}(\hat{\Phi}, \Xi, \hat{\Psi}, N_2)$ 
    converged = COMPAREOUTPUTTOTARGET(( $\boldsymbol{\theta}^{\{1\}}, \dots, \boldsymbol{\theta}^{\{N_2\}}$ ),  $\hat{\Phi}$ )
    while converged ≠ 1 do  $\triangleright$  Rerun contour volume estimation (if necessary modify
    vine copula KDE hyperparameters) and/or MCMC, with larger sample sizes if required
         $\hat{\Psi} = \text{CONTOURVOLUMEESTIMATOR}(\Xi, N'_1), N'_1 \geq N_1$ 
         $(\boldsymbol{\theta}^{\{1\}}, \dots, \boldsymbol{\theta}^{\{N'_2\}}) = \text{MCMC}(\hat{\Phi}, \Xi, \hat{\Psi}, N'_2), N'_2 \geq N_2$ 
        converged = COMPAREOUTPUTTOTARGET(( $\boldsymbol{\theta}^{\{1\}}, \dots, \boldsymbol{\theta}^{\{N'_2\}}$ ),  $\hat{\Phi}$ )
         $N_1 \leftarrow N'_1, N_2 \leftarrow N'_2$ 
    end while
    return  $(\boldsymbol{\theta}^{\{1\}}, \dots, \boldsymbol{\theta}^{\{N_2\}})$ 
end procedure

procedure SNAPSHOTESTIMATOR( $\mathbf{X}$ )  $\triangleright$  Fit snapshots with kernel density estimator
    (KDE)
     $\mathbf{X} \sim p(\mathbf{q}|\hat{\Phi})$ 
    return  $\hat{\Phi}$ 
end procedure

procedure CONTOURVOLUMEESTIMATOR( $\Xi, N_1$ )  $\triangleright$  Estimate volume of contours
    for  $i$  in  $1 : N_1$  do
         $\boldsymbol{\theta}^{\{i\}} \sim p(\boldsymbol{\theta}|\Xi)$   $\triangleright$  Sample from prior density
         $\mathbf{q}^{\{i\}} = \mathbf{q}(\boldsymbol{\theta}^{\{i\}})$   $\triangleright$  Calculate corresponding output value
    end for
     $(\mathbf{q}^{\{1\}}, \dots, \mathbf{q}^{\{N_1\}}) \sim p(\mathbf{q}|\hat{\Psi})$   $\triangleright$  Fit vine copula KDE
    return  $\hat{\Psi}$ 
end procedure

procedure MCMC( $\hat{\Phi}, \Xi, \hat{\Psi}, N_2$ )  $\triangleright$  Random Walk Metropolis algorithm targeting
    posterior parameter distribution
     $\boldsymbol{\theta}^{\{0\}} \sim \pi(\cdot)$   $\triangleright$  Sample from arbitrary initialisation distribution
    for  $i$  in  $1 : N_2$  do
         $\boldsymbol{\theta}^{\{i\}'} \sim \mathcal{N}(\boldsymbol{\theta}^{\{i-1\}}, \Sigma)$   $\triangleright$  Propose new parameter values
         $r = p(\boldsymbol{\theta}^{\{i\}'}|\Xi) p(\mathbf{q}(\boldsymbol{\theta}^{\{i-1\}})|\hat{\Psi}) p(\mathbf{q}(\boldsymbol{\theta}^{\{i\}'})|\hat{\Phi}) / [p(\boldsymbol{\theta}^{\{i-1\}}|\Xi) p(\mathbf{q}(\boldsymbol{\theta}^{\{i\}'})|\hat{\Psi}) p(\mathbf{q}(\boldsymbol{\theta}^{\{i-1\}})|\hat{\Phi})]$ 
         $u \sim U(0, 1)$   $\triangleright$  Sample from uniform distribution
        if  $r > u$  then
             $\boldsymbol{\theta}^{\{i\}} = \boldsymbol{\theta}^{\{i\}'}$   $\triangleright$  Accept proposal
        else
             $\boldsymbol{\theta}^{\{i\}} = \boldsymbol{\theta}^{\{i-1\}}$   $\triangleright$  Reject proposal
        end if
    end for
    return  $(\boldsymbol{\theta}^{\{1\}}, \dots, \boldsymbol{\theta}^{\{N_2\}})$ 
end procedure

procedure COMPAREOUTPUTTOTARGET(( $\boldsymbol{\theta}^{\{1\}}, \dots, \boldsymbol{\theta}^{\{N_2\}}$ ),  $\hat{\Phi}$ )  $\triangleright$  Check output
    distribution close to target
    for  $i$  in  $1 : N_2$  do
         $\tilde{\mathbf{q}}^{\{i\}} = \mathbf{q}(\boldsymbol{\theta}^{\{i\}})$   $\triangleright$  Compute QOIs for each parameter sample
    end for
    if  $p(\tilde{\mathbf{q}}) \approx p(\tilde{\mathbf{q}}|\hat{\Phi})$ ? then  $\triangleright$  Compare sampled output distribution with target
        return 1  $\triangleright$  If sufficiently close then converged
    else
        return 0
    end if
end procedure

```

To generate our results in §4, for the contour volume estimation step we assumed sample sizes were sufficient if the output samples from MCMC provided a reasonable approximation to the target, although we recognise that future work should refine this process further. For the MCMC step, we used adaptive covariance MCMC (see SOM of [22]) to sample from the target distribution, as it typically provides a considerable speed-up over Random Walk Metropolis [23, 24]. We also used the Gelman-Rubin convergence statistic, \hat{R} , to diagnose convergence [24, 25], with a convergence threshold of $\hat{R} \leq \sim 1.1$.

To solve the forward model of each differential equation, we used Julia’s inbuilt “solve” method for ODE models, which automatically chooses an efficient inbuilt solver [26].

4 Results

In this section, we use CMC to estimate posterior parameter distributions for three biological systems. In all but one of the examples, we assume that the first step of CMC (“SnapshotEstimator” within Algorithm 1) has already been completed, and we are faced with inferring a parameter distribution which, when mapped to outputs, recapitulates the target density. To accompany the text, we provide the Julia notebook used to generate the results. A table of priors used for each example is provided in Table 3.

4.1 Growth factor model

We first consider the “growth factor model” introduced by [12], which concerns the dynamics of inactive ligand-free cell surface receptors, R , and active ligand-bound cell surface receptors, P , modulated by an exogenous ligand, L . The governing dynamics are determined by the following system,

$$\frac{dR}{dt} = R_T k_{deg} + k_1 L R(t) + k_{-1} P(t) - k_{deg} R(t) \quad (13)$$

$$\frac{dP}{dt} = k_1 L R(t) - k_{-1} P(t) - k_{deg}^* P(t), \quad (14)$$

with initial conditions,

$$R(0) = 0.0, \quad P(0) = 0.0,$$

where $\boldsymbol{\theta} = (R_T, k_1, k_{-1}, k_{deg}, k_{deg}^*)$ are parameters to be determined. In this example, we use measurements of the active ligand-bound receptors P to estimate cellular heterogeneity in these processes. We denote the solution of eq. (14) as $P(t; \boldsymbol{\theta}, L)$ and seek to determine the parameter distribution consistent with an output distribution,

$$\mathbf{q} = \begin{pmatrix} q_1 \\ q_2 \end{pmatrix} = \begin{pmatrix} P(10; \boldsymbol{\theta}, 2) \\ P(10; \boldsymbol{\theta}, 10) \end{pmatrix} \sim \mathcal{N} \left[\begin{pmatrix} 2 \times 10^4 \\ 3 \times 10^4 \end{pmatrix}, \begin{pmatrix} 1 \times 10^5 & 0 \\ 0 & 1 \times 10^5 \end{pmatrix} \right]. \quad (15)$$

4.1.1 Uniform prior

To start, we specify a uniform prior for each of the five parameters, with bounds given in Table 3, and use CMC to estimate the posterior parameter distribution. In Figure 5A, we show the sampled outputs (blue points)

versus the contours of the target distribution (black solid closed curves), illustrating a good correspondence between the sampled and target densities. Above and to the right of the main panel, we also display the marginal target densities (solid black lines) versus kernel density estimator reconstructions of the output marginals from the CMC samples (dashed blue lines), which again highlights the fidelity of the CMC sampled density to the target.

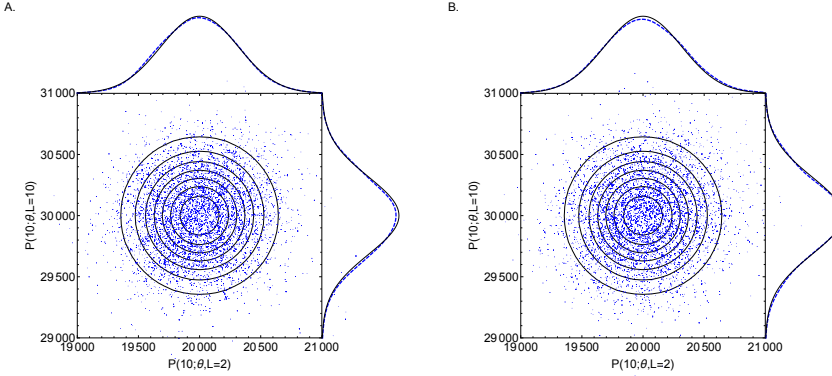


Figure 5: Growth factor model. Target joint output distribution (solid contour lines) and target marginal distributions (solid lines; above and to the right of each figure) versus outputs sampled by CMC (blue points) and reconstructed marginals (dashed lines). (A) uniform priors. (B) Gaussian priors. In CMC, 100,000 independent samples were used in the “ContourVolumeEstimator” step and 10,000 MCMC samples across each of 4 Markov chains were used in the second step, with the first half of the chains discarded as “warm-up” [24]. For the reconstructed marginal densities in the plots, we use Mathematica’s “SmoothKernelDistribution” function specifying bandwidths of 100 with Gaussian kernels [27].

In Figure 6A, we plot the joint posterior parameter distribution for k_1 , the rate of ligand binding to inactive receptors and k_{-1} , which dictates the rate of the reverse reaction. A given level of bound ligands can be generated in many different ways. Not surprisingly, it is the *ratio* of the forward and reverse reaction rates, k_1 and k_{-1} respectively, that is of greatest importance, and because of this, the distribution representing cell process heterogeneity contains linear positive correlations between these parameters.

In Figure 6B, we show the posterior parameter distribution for k_{deg} , the rate of degradation of ligand-free cell surface receptors and R_T , the rate of introduction of ligand-free cell surface receptors. This plot shows more concentrated posterior mass than in Figure 6A. Why can we better resolve (k_{deg}, R_T) compared to (k_1, k_{-1}) from our measurements? To answer this, it is useful to calculate the sensitivity of $P(t; \theta, L)$ to changes in each of the parameters. To account for the differing magnitudes of each parameter, we calculate elasticities, the proportional changes in measured output for a proportional change in parameter values, using the forward sensitivities method described in [28], and these are shown in Figure 7. When the exogenous ligand is set at $L = 2$, these indicate the active ligand-bound

receptor concentration is most elastic to changes in R_T and k_{deg} , meaning
 that their range is more restricted by the output measurement than for k_1
 and k_{-1} , which have much smaller elasticities at $t = 10$. In Table 2, we
 show the posterior quantiles for the estimated parameters, and in the last
 column, indicate the ratio of the 25%-75% posterior interval widths to the
 uniform prior range for each parameter. These were strongly negatively
 correlated with the magnitude of the elasticities for each parameter ($\rho =$
 0.95 , $t = -5.22$, $df = 3$, $p = 0.01$ for Pearson's product-moment correlation),
 indicating the utility of sensitivity analyses for optimal experimental design.
 We suggest, however, that CMC can also be used for this purpose, using
 synthetic data in place of real measurements.

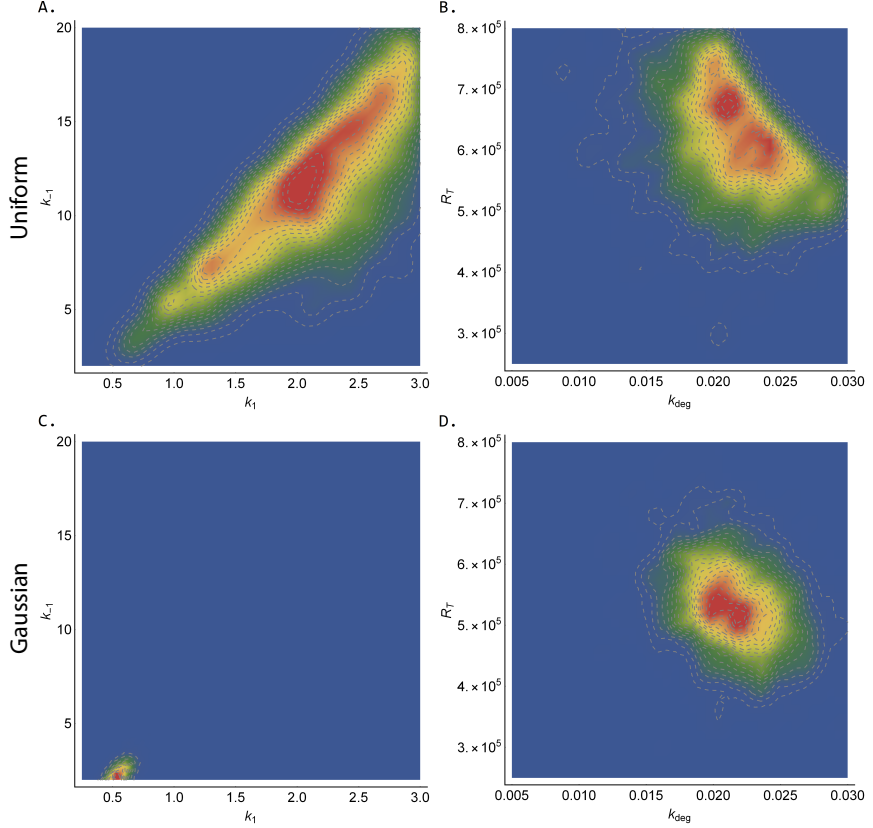


Figure 6: Growth factor model. Joint posterior distributions estimated by CMC. Top row (A-B): (k_1, k_{-1}) and (k_{deg}, R_T) using uniform priors. Bottom row (C-D): (k_1, k_{-1}) and (k_{deg}, R_T) using Gaussian priors. See Figure 5 caption for CMC details and Table 3 for the priors used. Red (blue) indicates areas of relatively high (low) probability density.

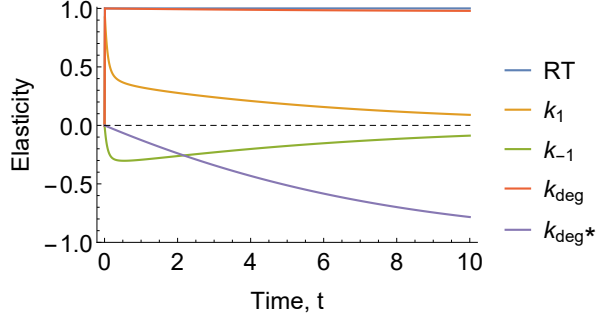


Figure 7: Growth factor model. Elasticities of the active ligand-bound receptors P with respect to each parameter as a function of time. When calculating the elasticities of each parameter, the other parameters were set to their posterior medians given in Table 2 and $L = 2$.

4.1.2 Gaussian prior

For an under-determined model, the number of QOIs, m , is less than the number of parameters, p , and there typically exists a non-singular set of parameter distributions mapping to the same target output distribution. To uniquely identify a posterior parameter distribution, it is, therefore, necessary to specify a prior parameter distribution. By incorporating priors, this also allows incorporation of pre-existing biological knowledge leading to reduced uncertainty in parameter estimates. CMC allows any prior with correct support to be used. Changes to priors affect both the “ContourVolumeEstimation” and “MCMC” steps of CMC (Algorithm 1), so that the (changed) posterior parameter distribution still maps to the target.

We now use CMC to estimate the posterior parameter distribution, when using Gaussian priors (prior hyperparameters shown in Table 3), which are more concentrated than the uniform priors used in §4.1.1. As desired, the target output distribution appears virtually unaffected by the change of priors (Figure 5B) although with substantial changes to the posterior parameter distribution (Figure 6C versus 6D). In particular, the marginal posterior distributions obtained from the Gaussian prior are narrower compared to the uniform case (rightmost column of Table 2). As in traditional Bayesian inference, prior choice has a greater influence on the posterior distribution when data provide less information on the underlying process. This is readily apparent in comparing the dramatic change from Figure 5A to 5C for (k_1, k_{-1}) , which have low sensitivities, with the more nuanced change from Figure 5B to 5D for (k_{deg}, R_T) , which have high sensitivities.

4.2 Michaelis-Menten kinetics

In this section, we use CMC to invert output measurements from the Michaelis-Menten model of enzyme kinetics (see, for example, [29]); illustrating the capability of CMC to resolve population substructure from multimodality of the output distribution. The Michaelis-Menten model of enzyme kinetics describes the dynamics of concentrations of an enzyme, E ,

375
376
377
378
379
380
381
382
383
384
385
386
387
388
389
390
391
392
393
394
395
396
397
398
399
400

Parameter	Quantiles					Posterior 25%-75% conc.
	2.5%	25%	50%	75%	97.5%	
Uniform prior						
R_T	441,006	548,275	606,439	677,055	772,484	23%
k_1	0.90	1.69	2.17	2.56	2.95	32%
k_{-1}	4.35	8.35	11.23	14.23	18.71	33%
k_{deg}	0.013	0.019	0.021	0.024	0.029	20%
k_{deg}^*	0.20	0.34	0.40	0.44	0.49	27%
Gaussian prior						
R_T	408,396	487,372	529,558	577,970	678,632	16%
k_1	0.39	0.49	0.54	0.60	0.70	4%
k_{-1}	1.39	1.92	2.26	2.63	3.35	4%
k_{deg}	0.016	0.020	0.022	0.024	0.027	16%
k_{deg}^*	0.22	0.29	0.33	0.38	0.46	21%

Table 2: **Growth factor model. Estimated quantiles from CMC samples with uniform and Gaussian priors.** The last column indicates the proportion of the uniform prior bounds occupied by the 25%-75% posterior interval in each case. The prior hyperparameters used in each case are given in Table 3.

a substrate, S , an enzyme-substrate complex, C , and a product, P ,

$$\begin{aligned} \frac{dE}{dt} &= -k_f E(t)S(t) + k_r C(t) + k_{cat}C(t), \\ \frac{dS}{dt} &= -k_f E(t)S(t) + k_r C(t), \\ \frac{dC}{dt} &= k_f E(t)S(t) - k_r C(t) - k_{cat}C(t), \\ \frac{dP}{dt} &= k_{cat}C(t), \end{aligned} \tag{16}$$

with initial conditions,

$$E(0) = E_0, S(0) = S_0, C(0) = C_0, P(0) = P_0, \tag{17}$$

where k_f is the rate of the forward reaction $E + S \rightarrow C$, k_r is the rate of the reverse reaction $C \rightarrow E + S$, and k_{cat} is the catalytic rate of product formation by the reaction $C \rightarrow E + P$.

4.2.1 Bimodal output distribution

When subpopulations of cells, each with distinct dynamics, are thought to exist, determining their characteristics - the proportions of cells in each cluster, their distinct parameter values, and so on - is often of key interest [15, 19]. Before formal inference occurs, multimodality of the output distribution may signal the existence of fragmented subpopulations of cells and to exemplify this we target a bimodal bivariate Gaussian distribution for measurements of the level of enzyme and substrate at $t = 1$ and $t = 2$

respectively,

420

$$\begin{aligned} \mathbf{q} = \begin{pmatrix} q_1 \\ q_2 \end{pmatrix} &= \begin{pmatrix} E(2.0; \boldsymbol{\theta}) \\ S(1.0; \boldsymbol{\theta}) \end{pmatrix} \sim p(\mathbf{q}; \boldsymbol{\mu}_1, \Sigma_1, \boldsymbol{\mu}_2, \Sigma_2) \\ &= \frac{1}{2} (\mathcal{N}(\mathbf{q}; \boldsymbol{\mu}_1, \Sigma_1) + \mathcal{N}(\mathbf{q}; \boldsymbol{\mu}_2, \Sigma_2)), \end{aligned} \quad (18)$$

where $\boldsymbol{\theta} = (k_f, k_r, k_{cat})$. The parameters of the Gaussian mixture components are,

$$\begin{aligned} \boldsymbol{\mu}_1 &= \begin{pmatrix} 2.2 \\ 1.6 \end{pmatrix}, \quad \Sigma_1 = \begin{pmatrix} 0.018 & -0.013 \\ -0.013 & 0.010 \end{pmatrix}, \\ \boldsymbol{\mu}_2 &= \begin{pmatrix} 2.8 \\ 1.0 \end{pmatrix}, \quad \Sigma_2 = \begin{pmatrix} 0.020 & -0.010 \\ -0.010 & 0.020 \end{pmatrix}. \end{aligned}$$

In what follows, we specify uniform priors on each element of $\boldsymbol{\theta}$ (see Table 3). Using a modest number of samples in each step, CMC well-approximates the output target distribution (Figure 8A). Without providing *a priori* information on the subpopulations of cells, two distinct clusters of cells emerged from application of CMC (orange and blue points in Figure 8B), each corresponding to distinct modes of the output distribution (corresponding coloured points in Figure 8A). It is worth noting, however, that the issues inherent with using MCMC to sample multimodal distributions similarly apply here. So, whilst adaptive MCMC [22] sufficed to explore this posterior surface, it may be necessary to use MCMC methods more robust to such geometries in other cases (for example, population MCMC [30]).

421
422
423
424
425
426
427
428
429
430
431

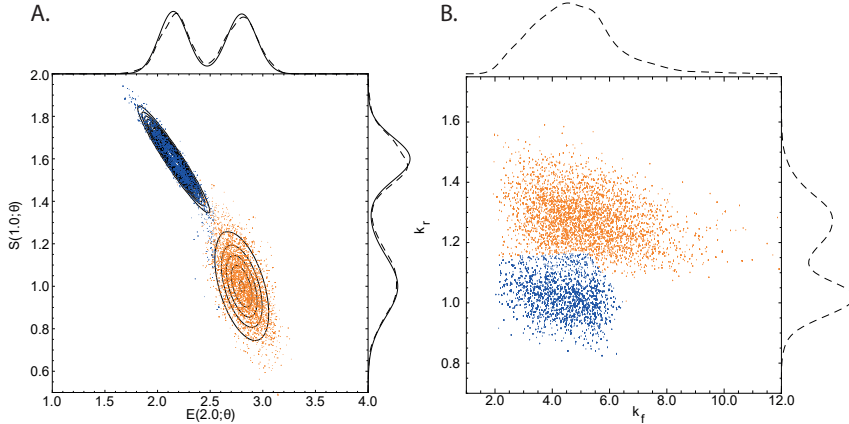


Figure 8: Michaelis-Menten model. (A) Bimodal target distribution q (solid contour lines) versus output samples (points). (B) posterior parameter samples (points). The solid and dashed lines above and to the side of panel A indicate the target and estimated marginal output distributions, respectively. In B, only estimated parameter marginals are shown as the exact solutions are unknown. The orange (blue) points in A were generated by the orange (blue) parameter samples in B. See Figure 5 caption for CMC details. Mathematica’s “SmoothKernelDistribution” function [27] with Gaussian kernels was used to construct marginal densities with: (A) default bandwidths, and (B) bandwidths of 0.3 (horizontal axis) and 0.03 (vertical axis). Mathematica’s “ClusteringComponents” function [27] was used to identify clusters in B.

4.2.2 Four-dimensional output distribution

432
433
434
435
436
437

Loos et al. (2018) consider a multidimensional output distribution, with correlations between system characteristics that evolve over time. Our approach allows arbitrary covariance structure between measurements, and to exemplify this, we now target a four-dimensional output distribution, with paired measurements of enzyme and substrate at $t = 1$ and $t = 2$,

$$\mathbf{q} = \begin{pmatrix} q_1 \\ q_2 \\ q_3 \\ q_4 \end{pmatrix} = \begin{pmatrix} E(1.0; \theta) \\ S(1.0; \theta) \\ E(2.0; \theta) \\ S(2.0; \theta) \end{pmatrix} \sim \mathcal{N} \left[\begin{pmatrix} 0.5 \\ 2.8 \\ 0.9 \\ 1.4 \end{pmatrix}, \begin{pmatrix} 0.02 & -0.05 & 0.04 & -0.05 \\ -0.05 & 0.30 & -0.15 & 0.20 \\ 0.04 & -0.15 & 0.12 & -0.17 \\ -0.05 & 0.20 & -0.17 & 0.30 \end{pmatrix} \right]. \quad (19)$$

Since this target has four QOIs, and the Michaelis-Menten model has three rate parameters (k_f, k_r, k_{cat}), the system is over-identified and so CMC cannot be straightforwardly applied. Instead, we allow the four initial states (E_0, S_0, C_0, P_0) to be uncertain quantities, bringing the total number of parameters to seven. We set uniform priors on all parameters (see Table 3). In order to check that the model and priors were consistent with the output distribution given by eq. (19), we plotted the output measurements used to estimate contour volumes (in the first step of the “ContourVolumeEstimator” method in Algorithm 1) against the target (Figure 9). Since the main support of the densities (black contours) lies within a region of output space reached by independent sampling of the priors (blue points), this indicated the target could feasibly be generated from this model and priors, and we proceeded to estimation by CMC.

438
439
440
441
442
443
444
445
446
447
448
449
450

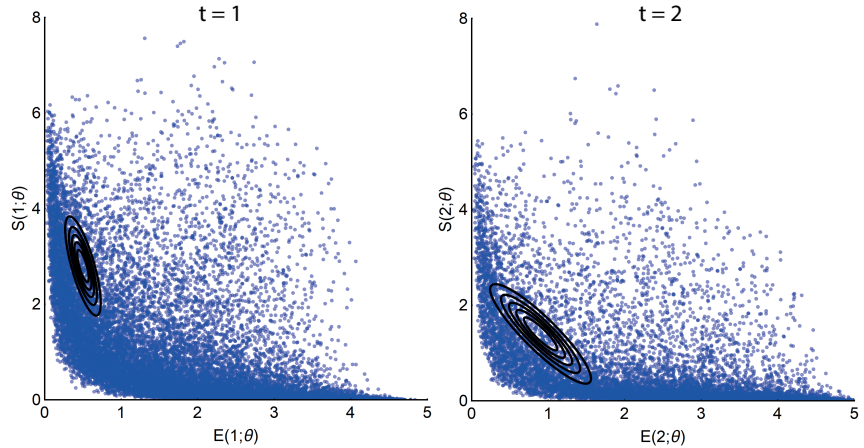


Figure 9: Michaelis-Menten model. QOIs (blue points) obtained by independently sampling the priors versus the target distribution (black solid contours). Left: (q_1, q_2) . Right: (q_3, q_4) . We show 20,000 output samples, where each set of four measurements was obtained from a single sample of all parameters. The output target distribution shown by the contours corresponds to the marginal densities of each pair of enzyme-substrate measurements given by eq. (19).

Figure 10 plots the output samples of enzyme and substrate from the last step of CMC for $t = 1$ (blue points) and $t = 2$ (orange points) versus the contours (black lines) of the joint marginal distributions of eq. (19). The distribution of paired enzyme-substrate samples illustrates that the CMC output distribution approximates the target density, itself representing dynamic evolution of the covariance between enzyme and substrate measurements. Target marginal distributions (solid lines) along with their approximations from kernel density estimation (dashed lines) are also shown above and to the right of the main panel of Figure 10 and largely indicate correspondence.

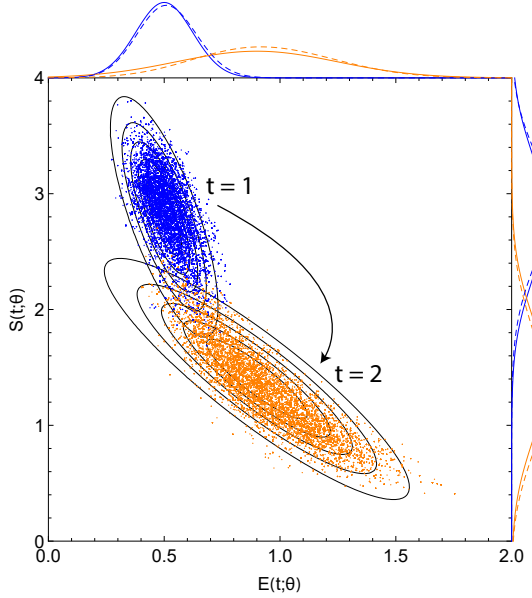


Figure 10: Michaelis-Menten model. Posterior output samples from CMC (coloured points) versus contour plots (black solid lines) of the joint marginal distributions of eq. (19). Enzyme and substrate measurements are given by the horizontal and vertical axes, respectively. Output functionals for (q_1, q_2) and (q_3, q_4) are given by blue and orange points, respectively. The solid and dashed coloured lines outside the panels indicate exact target marginals of eq. (19) and those estimated by CMC, respectively. In the ‘‘ContourVolumeEstimator’’ step, 200,000 independent samples were used, and in the MCMC step, 10,000 samples across each of 4 Markov chains were used, with the first half of the chains discarded as ‘‘warm-up’’ [24]. Mathematica’s ‘‘SmoothKernelDistribution’’ function, using Gaussian kernels [27] and bandwidths ranging from 0.1 to 0.4, was used to reconstruct marginal densities.

4.3 TNF signalling pathway

We now illustrate how CMC can be applied to an ODE system of larger size, the tumour necrosis factor (TNF) signalling pathway model introduced in [31] and used by [15] to illustrate a Bayesian approach to cell population variability estimation. The model incorporates known activating and inhibitory interactions between four key species within the TNF pathway: active caspase 8, x_1 , active caspase 3, x_2 , a nuclear transcription factor, x_3

and its inhibitor, x_4 , such that

$$\begin{aligned}\frac{dx_1}{dt} &= -x_1(t) + \frac{1}{2} [\beta_4(x_3(t))\alpha_1(u(t)) + \alpha_3(x_2(t))] \\ \frac{dx_2}{dt} &= -x_2(t) + \alpha_2(x_1(t))\beta_3(x_3(t)) \\ \frac{dx_3}{dt} &= -x_3(t) + \beta_2(x_2(t))\beta_5(x_4(t)) \\ \frac{dx_4}{dt} &= -x_4(t) + \frac{1}{2} [\beta_1(u(t)) + \alpha_4(x_3(t))],\end{aligned}\tag{20}$$

with initial conditions,

$$x_1(0) = 0.0, \quad x_2(0) = 0.0, \quad x_3(0) = 0.29, \quad x_4(0) = 0.625.\tag{21}$$

The functions α_i and β_j represent activating and inhibitory interactions respectively,

$$\begin{aligned}\alpha_i(z) &= \frac{z^2}{a_i^2 + z^2}, \quad i = 1, \dots, 4, \\ \beta_j(z) &= \frac{b_j^2}{b_j^2 + z^2}, \quad j = 1, \dots, 5,\end{aligned}\tag{22}$$

and the parameters a_i for $i \in (1, 2, 3, 4)$ and b_j for $j \in (1, 2, 3, 4, 5)$ represent activation and inhibition thresholds. The function $u(t)$ represents a TNF stimulus represented by a top hat function,

$$u(t) = \begin{cases} 1, & \text{if } t \in [0, 2]. \\ 0, & \text{otherwise.} \end{cases}\tag{23}$$

In under-determined models, a non-zero-volume set of parameters can produce the same output values. A consequence of this unidentifiability is that we cannot perform “full circle” inference: that is, using a known parameter distribution to generate an output distribution does not result in that parameter distribution being recovered through inference. We illustrate this idea by generating an output distribution by varying a single parameter value between runs of the forward model (20) and performing inference on all nine system parameters, whilst collecting only two output measurements. Specifically, we randomly sample $a_1 \sim \mathcal{N}(0.6, 0.05)$ for each simulation of the forward model, whilst holding the other parameters constant,

$$(a_2, a_3, a_4, b_1, b_2, b_3, b_4, b_5) = (0.2, 0.2, 0.5, 0.4, 0.7, 0.3, 0.5, 0.4),$$

and measure $q_1 = x_1(2.0)$ and $q_2 = x_2(1.0)$ in each case. In doing so, we obtain an output distribution well-approximated by the bivariate Gaussian distribution,

$$\begin{aligned}\mathbf{q} &= \begin{pmatrix} q_1 \\ q_2 \end{pmatrix} = \begin{pmatrix} x_1(2.0) \\ x_2(1.0) \end{pmatrix} \\ &\sim \mathcal{N} \left[\begin{pmatrix} 0.26 \\ 0.07 \end{pmatrix}, \begin{pmatrix} 2.1 \times 10^{-4} & 5.9 \times 10^{-5} \\ 5.9 \times 10^{-5} & 1.8 \times 10^{-5} \end{pmatrix} \right].\end{aligned}\tag{24}$$

We now apply CMC to the target output distribution given by eq. (24) to estimate a posterior distribution over all nine parameters of eq. (20). Apart than for a few cases, the priors for each parameter were chosen to *exclude* the values that were used to generate the output distribution (see

Table 3), to illustrate the non-equivalence between the recovered posterior distribution and the data generating process. In Figure 11A, we plot the actual parameter values (horizontal axis) used to generate the data versus the estimated values (vertical axis). This illustrates that, due to the chosen priors, there is a disjunction between actual and estimated parameter values in all cases apart from a_1 . Because the model is under-determined, however, the corresponding output distribution well approximates the target despite these differences (Figure 11B).

482
483
484
485
486
487
488
489

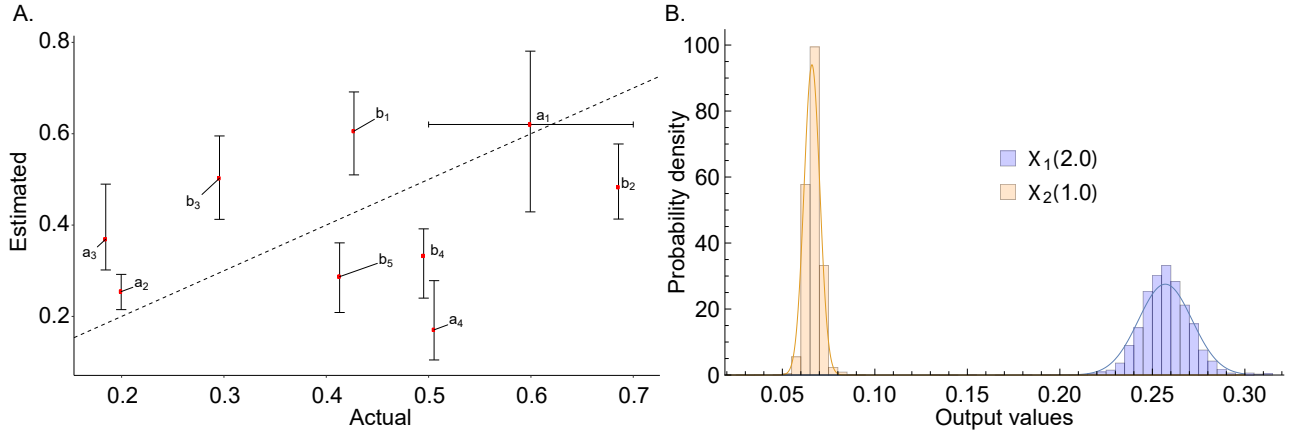


Figure 11: **TNF signalling pathway model.** (A) Actual parameter values versus estimated quantiles for the output distribution of eq. (24). (B) Marginal output targets (solid lines) and sampled output distributions (histograms). In A, in the vertical direction, red points indicate 50% posterior quantiles and upper and lower whiskers indicate 97.5% and 2.5% quantiles, respectively; in the horizontal direction, with the exception of a_1 , red points indicate the parameter values used to generate the data; for a_1 , the red point indicates the mean of the Gaussian distribution used to generate the data and the whiskers indicate its 95% quantiles. In CMC, 10,000 independent samples were used in the “ContourVolumeEstimator” step and 5,000 MCMC samples across each of 4 Markov chains were used in the second, with the first half of the chains discarded as “warm-up” [24].

Cell populations may be well described by subpopulations that each evolve along characteristic trajectories over time. We now apply CMC to investigate a bimodal output distribution for the TNF signalling pathway model similar to that investigated by [15]. We aim to estimate the posterior parameter distribution mapping to the following output distribution,

$$\mathbf{q} = \begin{pmatrix} q_1 \\ q_2 \\ q_3 \end{pmatrix}, \quad (25)$$

where,

$$\begin{aligned} q_1 &= \mathbf{x}_2(1.0) \sim \mathcal{N}(0.06, 0.01) \\ q_2 &= \mathbf{x}_2(2.0) \sim \frac{1}{2} (\mathcal{N}(0.1, 0.01) + \mathcal{N}(0.14, 0.01)) \\ q_3 &= \mathbf{x}_2(4.0) \sim \frac{1}{2} (\mathcal{N}(0.1, 0.01) + \mathcal{N}(0.20, 0.01)), \end{aligned} \quad (26)$$

490
491
492
493
494

where the target distributions for $q_2(2.0)$ and $q_2(4.0)$ indicate mixtures
 496 of univariate Gaussians, and the priors used are given in Table 3. This
 497 target distribution, along with the unique trajectories obtained by applying
 498 the CMC algorithm, are shown in Figure 12. This figure illustrates that
 499 the bimodality of the output distribution means CMC samples clusters of
 500 parameter values without the need for subpopulation information to be
 501 provided ahead of estimation.
 502

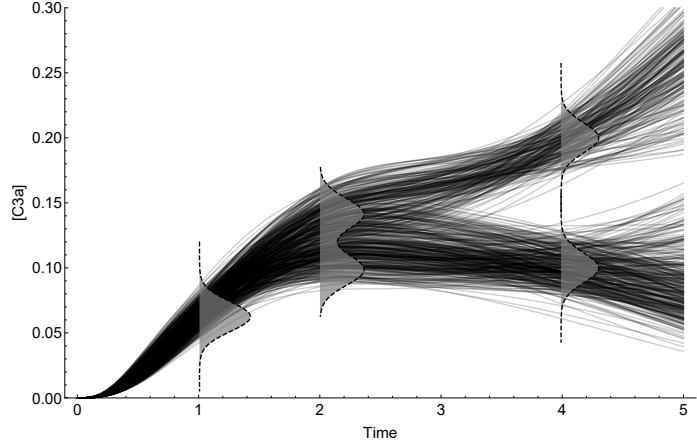


Figure 12: TNF signalling pathway model. Target output distribution (dashed plots with grey filling) and unique trajectories (black solid lines) obtained from the posterior parameter distribution. In CMC, 10,000 independent samples were used in the “ContourVolumeEstimator” step and 5,000 MCMC samples across each of 4 Markov chains were used in the second, with the first half of the chains discarded as “warm-up” [24].

Model	Target density	Parameter	Prior density	Prior p_1	Prior p_2
Growth factor	2D Gaussian	R_T	uniform	2.5×10^5	8×10^5
		k_1	uniform	0.25	3.0
		k_{-1}	uniform	2.0	20.0
		k_{deg}	uniform	0.005	0.03
		k_{deg}^*	uniform	0.1	0.5
Growth factor	2D Gaussian	R_T	Gaussian	5×10^5	1×10^5
		k_1	Gaussian	0.5	0.1
		k_{-1}	Gaussian	3.0	1.0
		k_{deg}	Gaussian	0.02	0.005
		k_{deg}^*	Gaussian	0.3	0.1
Michaelis-Menten	bimodal Gaussian	k_f	uniform	0.2	15
		k_r	uniform	0.2	2.0
		k_{cat}	uniform	0.5	3.0
Michaelis-Menten	4D Gaussian	k_f	uniform	0.2	15
		k_r	uniform	0.2	2.0
		k_{cat}	uniform	0.2	3.0
		E_0	uniform	3.0	5.0
		S_0	uniform	5.0	10.0
		C_0	uniform	0.0	0.2
TNF signalling	bivariate Gaussian	P_0	uniform	0.0	0.2
		a_1	uniform	0.4	0.8
		a_2	uniform	0.1	0.7
		a_3	uniform	0.3	0.7
		a_4	uniform	0.1	0.3
		b_1	uniform	0.5	0.7
		b_2	uniform	0.4	0.6
		b_3	uniform	0.4	0.6
		b_4	uniform	0.2	0.4
		b_5	uniform	0.2	0.4
TNF signalling	bimodal Gaussian	a_1	uniform	0.5	0.7
		a_2	uniform	0.1	0.3
		a_3	uniform	0.1	0.3
		a_4	uniform	0.4	0.6
		b_1	uniform	0.3	0.5
		b_2	uniform	0.6	0.8
		b_3	uniform	0.2	0.4
		b_4	uniform	0.4	0.6
		b_5	uniform	0.3	0.5

Table 3: **Priors used for each problem in §4.** The parameters p_1 and p_2 indicate the prior hyperparameters: for uniform priors, these correspond to the lower and upper limits; for Gaussian priors, they correspond to the mean and standard deviation.

5 Discussion

Determining the cause of variability in cellular processes is crucial in many applications, ranging from bioengineering to drug development. In this

504
505

paper, we introduce a Bayesian method for estimating cellular heterogeneity from “snapshot” measurements of cellular properties, taken at discrete intervals during experiments. Our approach assumes what we call a “heterogeneous ordinary differential equation” (HODE) framework, in which biochemical processes in all cells are governed by a common ODE. Each cell, however, has different rate parameter values, causing a variety of measurements to be obtained across cells. In this framework, estimating heterogeneity in cellular processes amounts to determining the probability distributions of parameter values of the governing ODE. Our method of estimation is a two-step Monte Carlo sampling process we term “Contour Monte Carlo” (CMC), which does not require cell population substructure to be provided before estimation, unlike for other approaches. CMC can be used to process high volumes of individual cellular measurements since the framework involves fitting a kernel density estimator to raw experimental data and using these distributions rather than data as the target outcome. CMC also allows arbitrary multivariate structure in the measurement space meaning it can capture correlations between the same cellular species at different timepoints or, for example, contemporaneous correlations between different cellular compartments. Being a Bayesian approach, CMC uses prior distributions over parameter values to ensure uniqueness of the posterior distribution, allowing pre-experimental knowledge to be used to improve estimation robustness. The flexible and robust framework that CMC provides means it can be used to perform automatic inference for wide-ranging systems of practical interest.

Our approach also provides a natural way to test that the process is working satisfactorily. Feeding the posterior parameter samples obtained by CMC into forward model simulations results in a distribution of output values, which can be compared to the target. Indeed, we have found this comparison indispensable in applying CMC in practice and include it as the last step in the CMC algorithm (Algorithm 1). Discrepancies between the target output distribution and samples from it by CMC can occur either as a result of poor estimates of the “contour volume distribution” in the first stage of the algorithm or due to insufficient MCMC samples in the second. Either of these issues are often easily addressed by increasing sample sizes or changing hyperparameter settings for the kernel density estimator. Although kernel density estimation in high dimensional spaces remains an open research problem, we have found vine copula kernel density estimation works well for the dimensionality of output measurements we investigate here [21].

Failure to reproduce a given output distribution can also indicate that the generating model (the priors and the forward model) are incongruent with experimental results. This may either be due to misspecification of the ODE system or because the assumption of a deterministic forward model is inappropriate. Our approach currently assumes that output variation is dominated by cellular variation in the parameter values of the underlying ODE, with measurement noise making a negligible contribution. Whether this is a reasonable assumption depends on the system under investigation and, more importantly, on experimental details. We recognise that neglecting measurement noise when it is an important determinant of the observed data means CMC will overstate cellular variation. It may also mean that some output distributions cannot be obtained by our model system (i.e. HODEs without noise). Future work incorporating a stochastic noise process or, more generally, including stochastic cellular mechanisms

is thus likely to be worthwhile. 559
We have labelled our approach as Bayesian since it involves explicit 560
estimation of probability distributions and requires priors. We recognise, 561
however, that it is not of the form used in traditional Bayesian inference. 562
This is because rather than aiming to formulate a model that describes 563
output observations, our approach aims to recapitulate output *distributions*. 564
Others [32], (including us [20]), have considered similar problems before; 565
perhaps most notably by Albert Tarantola in his landmark work on inverse 566
problem theory (see, for example, [33]), which has generated considerable 567
interest in areas such as the geosciences [34, 35]. In Tarantola’s framework, 568
a joint input parameter and output space is considered, where prior knowl- 569
edge and experimental theory combine elegantly to produce a posterior 570
distribution whose marginal output distribution is a weighted “conjunction” 571
of various sources of information. This work has seen considerable interest 572
in areas such as the geosciences [34, 35], and we propose that Tarantola’s 573
approach may prove useful for the biosciences. 574

The natural world is rife with variation, and mathematical models 575
represent frameworks for understanding its causes. Typically, the state of 576
biological knowledge is such that one effect, a given pattern of variation, 577
has many possible causes. Observational or experimental data can be used 578
to apportion weight to each cause, in a process that amounts to solving 579
an inverse problem. The approach we describe here follows the Bayesian 580
paradigm of inverse problem solving where uncertainty in potential causes 581
(i.e. parameter values) is described using probability distributions. Here, 582
we illustrate the worth of our method by using it to estimate cellular 583
heterogeneity in biochemical processes, however, it could equally be used to 584
invert other classes of under-determined systems arising elsewhere. Contour 585
Monte Carlo provides an automatic framework for performing inference on 586
such under-determined systems and the use of priors allows for robust and 587
precise parameter estimation unattainable through the data alone. 588

6 Author contributions

BL, DJG and SJT conceived the study. BL carried out the analysis. All 589
authors helped to write and edit the manuscript. 590
591

References

- [1] M Ridley. *The red queen: sex and the evolution of human nature.* Penguin UK, 1994.
- [2] D Fraser and M Kaern. A chance at survival: gene expression noise and phenotypic diversification strategies. *Molecular Microbiology*, 71(6):1333–1340, 2009.
- [3] F Delvigne, Q Zune, AR Lara, W Al-Soud, and SJ Sørensen. Metabolic variability in bioprocessing: implications of microbial phenotypic heterogeneity. *Trends in Biotechnology*, 32(12):608–616, 2014.
- [4] RA Gatenby, K Smallbone, PK Maini, F Rose, J Averill, Raymond B Nagle, L Worrall, and RJ Gillies. Cellular adaptations to hypoxia and acidosis during somatic evolution of breast cancer. *British Journal of Cancer*, 97(5):646, 2007.

- [5] PM Altrock, LL Liu, and F Michor. The mathematics of cancer: integrating quantitative models. *Nature Reviews Cancer*, 15(12):730, 2015.
- [6] SJ Altschuler and LF Wu. Cellular heterogeneity: do differences make a difference? *Cell*, 141(4):559–563, 2010.
- [7] MB Elowitz, AJ Levine, ED Siggia, and PS Swain. Stochastic gene expression in a single cell. *Science*, 297(5584):1183–1186, 2002.
- [8] HH Chang, M Hemberg, M Barahona, DE Ingber, and S Huang. Transcriptome-wide noise controls lineage choice in mammalian progenitor cells. *Nature*, 453(7194):544, 2008.
- [9] S Waldherr. Estimation methods for heterogeneous cell population models in systems biology. *Journal of The Royal Society Interface*, 15(147):20180530, 2018.
- [10] R Erban, J Chapman, and P Maini. A practical guide to stochastic simulations of reaction-diffusion processes. *arXiv preprint arXiv:0704.1908*, 2007.
- [11] D Ramkrishna and MR Singh. Population balance modeling: current status and future prospects. *Annual Review of Chemical and Biomolecular Engineering*, 5:123–146, 2014.
- [12] P Dixit, E Lyashenko, M Niepel, and D Vitkup. Maximum entropy framework for inference of cell population heterogeneity in signaling network dynamics. *bioRxiv*, page 137513, 2018.
- [13] WG Telford, T Hawley, F Subach, V Verkhusha, and RG Hawley. Flow cytometry of fluorescent proteins. *Methods*, 57(3):318–330, 2012.
- [14] AJ Hughes, DP Spelke, Z Xu, CC Kang, DV Schaffer, and AE Herr. Single-cell western blotting. *Nature Methods*, 11(7):749, 2014.
- [15] J Hasenauer, S Waldherr, M Doszczak, N Radde, P Scheurich, and F Allgöwer. Identification of models of heterogeneous cell populations from population snapshot data. *BMC Bioinformatics*, 12(1):125, 2011.
- [16] O Hilsenbeck, M Schwarzfischer, S Skylaki, B Schauberger, PS Hoppe, D Loeffler, KD Kokkaliaris, S Hastreiter, E Skylaki, A Filipczyk, et al. Software tools for single-cell tracking and quantification of cellular and molecular properties. *Nature Biotechnology*, 34(7):703, 2016.
- [17] FSO Fritzsch, C Dusny, O Frick, and A Schmid. Single-cell analysis in biotechnology, systems biology, and biocatalysis. *Annual Review of Chemical and Biomolecular Engineering*, 3:129–155, 2012.
- [18] J Hasenauer, C Hasenauer, T Hucho, and FJ Theis. ODE constrained mixture modelling: a method for unraveling subpopulation structures and dynamics. *PLOS Computational Biology*, 10(7):e1003686, 2014.
- [19] C Loos, K Moeller, F Fröhlich, T Hucho, and J Hasenauer. A hierarchical, data-driven approach to modeling single-cell populations predicts latent causes of cell-to-cell variability. *Cell Systems*, 6(5):593–603, 2018.

- [20] B Lambert, D Gavaghan, and SJ Tavener. Inverse sensitivity analysis of mathematical models avoiding the curse of dimensionality. *BioRxiv*, page 432393, 2018.
- [21] T Nagler and C Czado. Evading the curse of dimensionality in non-parametric density estimation with simplified vine copulas. *Journal of Multivariate Analysis*, 151:69–89, 2016.
- [22] RH Johnstone, ETY Chang, R Bardenet, TP De Boer, DJ Gavaghan, P Pathmanathan, RH Clayton, and GR Mirams. Uncertainty and variability in models of the cardiac action potential: can we build trustworthy models? *Journal of Molecular and Cellular Cardiology*, 96:49–62, 2016.
- [23] N Metropolis, AW Rosenbluth, MN Rosenbluth, AH Teller, and E Teller. Equation of state calculations by fast computing machines. *The Journal of Chemical Physics*, 21(6):1087–1092, 1953.
- [24] B Lambert. *A Student’s Guide to Bayesian Statistics*. Sage Publications Ltd., 2018.
- [25] A Gelman and DB Rubin. Inference from iterative simulation using multiple sequences. *Statistical Science*, pages 457–472, 1992.
- [26] J Bezanson, A Edelman, S Karpinski, and VB Shah. Julia: A fresh approach to numerical computing. *SIAM Review*, 59(1):65–98, 2017.
- [27] Inc. Wolfram Research. Mathematica 8.0. <https://www.wolfram.com>.
- [28] AC Daly, DJ Gavaghan, J Cooper, and SJ Tavener. Inference-based assessment of parameter identifiability in nonlinear biological models. *Journal of The Royal Society Interface*, 15, 2018.
- [29] JD Murray. *Mathematical biology: I. An Introduction (interdisciplinary applied mathematics)(Pt. 1)*. New York, Springer, 2007.
- [30] A Jasra, DA Stephens, and CC Holmes. On population-based simulation for static inference. *Statistics and Computing*, 17(3):263–279, 2007.
- [31] M Chaves, T Eissing, and F Allgower. Bistable biological systems: a characterization through local compact input-to-state stability. *IEEE Transactions on Automatic Control*, 53(Special Issue):87–100, 2008.
- [32] T Butler, J Jakeman, and T Wildey. Combining push forward measures and baye’s rule to construct consistent solutions to stochastic inverse problems. *SIAM J. Sci. Comput.*, 40(2):A984–A1011, 2018.
- [33] A Tarantola. *Inverse problem theory and methods for model parameter estimation*, volume 89. SIAM, 2005.
- [34] K Mosegaard and A Tarantola. Monte Carlo sampling of solutions to inverse problems. *Journal of Geophysical Research: Solid Earth*, 100(B7):12431–12447, 1995.
- [35] T Vukicevic and D Posselt. Analysis of the impact of model nonlinearities in inverse problem solving. *Journal of the Atmospheric Sciences*, 65(9):2803–2823, 2008.